Incipient Motion Behavior of the Settled Particles in Supercritical CO_2

Lei Hou [a,b,d*], Xiaobing Bian [a,b], Xueyu Geng [c], Baojiang Sun [d*], Honglei Liu [a,b], Wenfeng Jia [a,b]

[a] State Key Laboratory of Shale Oil and Gas Enrichment Mechanisms and Effective Development, Beijing 100101, China;
[b] SINOPEC Research Institute of Petroleum Engineering, Beijing 100101, China;
[c] School of Engineering, The University of Warwick, Coventry CV4 7AL, UK
[d] School of Petroleum Engineering, China University of Petroleum (East China), 266580, China;

Abstract

The incipient motion process of settled particles in supercritical CO_2 was studied through experimental measurements and force analyses. By referring to the theories of sand-wind and sediment restarting, the incipient motion state description and mechanism were optimized to fill the theoretical gaps in particle restarting research in the petroleum industry. Visualization experiments were carried out under various temperature, pressure, and particle conditions. The critical pump rates for the onset of grain motion in supercritical CO_2 were measured. A critical pump rate empirical formula was obtained based on the experimental results and a derived Shields number expression. The average critical Shields number in supercritical CO_2 was 0.0028. The cohesive force on particles is zero in supercritical CO_2 based on its non-interfacial-tension characteristic. The measured spinning rate of the restarting particles in supercritical CO_2 was 121 r/s on average. Therefore, the calculated value of the Magnus force was approximately 30% of the force of gravity on particle. Particle incipient motion in supercritical CO_2 has a varying driving force (Magnus force) and simple resistant force (lack of cohesive force), which enhances the incipient motion of particles in supercritical CO_2.

Keywords: supercritical CO_2; particle incipient motion; visualization experiments; Shields number; Magnus force

Corresponding authors. Tel.: + 86 18610062455; +86 532 86983137
E-mail address: wto511@126.com (Lei Hou); sunbj1128@126.com (Baojiang Sun)

1. Introduction

Supercritical CO_2 (SC-CO_2), a new environmentally friendly operating fluid, has potentially wide applications in the petroleum industry. For example, it can be used as a fracturing and drilling fluid. One of the primary applications of SC-CO_2 application is the solid particle transportation, including the transportation of fracturing proppants and drilling cuttings [1–3]. However, the low viscosity (as low as gases) and high density (as high as liquid) of SC-CO_2 obscure its particle transportation capability. Viscosity is typically used as the criterion for particle transportation in previous studies [4–7]. Therefore, the particle transportation capability of SC-CO_2 is generally considered to be too low for efficient operation, which has become one of the main restraining factors for SC-CO_2 application in petroleum engineering.

Previous studies have revealed that particles are transported in hierarchical form in low-viscosity fluids. For example, the proppants are transported by water or slick-water during fracturing. Drilling cuttings tend to heap up in cutting beds in the horizontal wells. The solid phase experiences settling, accumulation, restarting, and suspension during the migration process [8, 9]. The restarting process of the settled particles is one of the key links that can be used as a criterion for particle transportation capability [10]. Therefore, we studied the particle incipient motion behavior of settled particles in SC-CO_2.

The theories of sand dynamics and river sediment dynamics were introduced into the petroleum engineering field to fill in the theoretical gaps because little research has been performed specifically on the description of the particle restarting status and mechanism in the petroleum industry [11–14]. The description of the particle restarting status was used as a criterion during our experiments and the particle restarting mechanism was used for numerical analysis.

For description of the particle restarting status, the Karmer [15] method is widely used, where the restarting status is divided into four levels according to particle motion and the scale of restarting particles: non-particle restarting, slight particle restarting, moderate particle restarting, and general particle restarting. Ouriemi [16] analyzed the unsteadiness of the initial sand banks. Particles on the surface tend to readjust to a steadier status, which has the appearance of slight particle restarting. Therefore, the moderate particle restarting status was chosen as the criterion for our experiments by synthesizing the Karmer and Ouriemi theories. When a considerable number of particles with medium sizes on a bank surface begin to move and the shape of the bank remains the same, the moderate particle restarting status is achieved. At this time, various parameters, such as pump rate, temperature, pressure, height of the bank, and particle motion parameters, were recorded during our experiments and used to fit the critical pump rate for particle restarting in SC-CO_2.

There are four main aspects of the particle restarting mechanism: rolling, striking, differential pressure, and slope [11]. In the case of petroleum engineering (fracturing or drilling), the proppants or drill cuttings are transported in the form of a two-phase flow. Therefore, the settled particles are continuously struck by moving particles. Proppants have good sphericity and roll easily based on the force of the flowing liquid. Therefore, the striking and rolling theories suit the restarting process for proppants and drill cuttings in petroleum engineering. The striking theory primarily focuses on the energy exchange between particles. This paper focuses on the particle transportation capability of SC-CO_2. Therefore, the rolling theory was used in our numerical analysis to identify the restarting behavior in SC-CO_2.

Visualization experiments were conducted to record the entire process of the particle restarting.

Quantitative evaluation and analysis were carried out to gain a better understanding of particle restarting conditions and behaviors in SC-CO_2. Additionally, a critical restarting condition empirical formula was fitted.

2. Material and methods

2.1 Materials

Ceramic proppants, which are used for propping open fractures during hydraulic fracturing, were selected for their uniform density and sphericity. A conventional proppant, with a density of 3120 kg/m^3, and a lightweight proppant, with a density of 2630 kg/m^3, were used for our experiments. The diameters of the particles fall in the range from 0.3 mm to 0.85 mm. The proppants were obtained from the Down-hole Service Co. at the Shengli Oil Field (SINOPEC). CO_2 with a purity of 99.99% was purchased from the Tianyuan Gas Product Co. (Qingdao, China).

2.2 Apparatus and procedures

A self-designed visualization apparatus was developed for particle restarting experiments in SC-CO_2. The apparatus consists of a visualization channel simulator and a high-speed camera system, as shown in Figure 1. The channel simulator consists of four identical units. Each unit has a length of 250 mm. The simulated channel has a fixed width of 5 mm and a height of 50 mm. There are two pairs of observation windows in each unit. The windows have a thickness of 50 mm, which allows them to withstand pressures as high as 30 MPa. They have a diameter of 46 mm, which covers nearly the entire height of the channel. The high-speed camera is an OLYMPUS i-SPEED TR. It has a maximum resolution of 1280 × 1024 pixels at a frame rate of 2000 fps. The light source (SHIBUYA JHP-40WP) is an LED cold-light illuminator that does not affect the temperature of the SC-CO_2 in the stimulated channel. The temperature sensor (Pt 100) was

manufactured by the JIMMING Instrument Co, Ltd., and its accuracy was 0.1 ℃. The pressure sensor (Baissde 701) was manufactured in the USA, and its accuracy was 0.075 MPa. The mass flow meter (DMF-1-4) was manufactured by the Beijing Sincerity Automatic Equipment Co., Ltd, and its accuracy was 0.2 %. CO_2, under supercritical conditions is supplied by a circulating platform. Additional details regarding the platform can be found in [17].

During the experimental process, the high-speed camera system was placed on both sides of the third window from the SC-CO_2 inlet to eliminate the boundary effects. First, a mixture of SC-CO_2 and proppant particles was injected into the channel. A sand bank then formed based on the accumulation of the settled particles, as shown in Figure 2. Next, pure SC-CO_2 was injected into the channel to restart the particles on sand bank surface. When the particles achieved the moderate restarting status, the high-speed camera recorded the incipient motions of the moving particles. The temperature, pressure, and flow rate were all recorded. The experimental data were processed using the OLYMPUS i-SPEED control software. The average uncertainty of the parameters measured by the experimental apparatus is 0.19% [18].

3. Results and discussion

3.1 Experimental results

Nine groups of experiments were carried out under various temperature, pressure, and particle conditions, as listed in Table 1. It is important to note that the sand banks were heaped up naturally. Therefore, the heights of the sand banks were random in nature. The higher the sand bank, the smaller the remaining channel space. A smaller channel space results in a higher flow rate and better particle transportation capability of SC-CO_2 at the same pump rate. Therefore, the restarting pump rates (the pump rate at which particle restarting occurs) in Table 1 list a wide range

corresponding to the various heights of the sand banks.

The fourth group of experiments in Table 1 is taken as an example to illustrate the experimental foundation and data processing procedure. For this group, the temperature and pressure of the SC-CO_2 were 42.7 °C and 9.42 MPa, respectively. The data regarding the particle restarting moment captured by the high-speed camera are shown in Figure 3. One can see that a significant number of particles with medium sizes on the sand bank surface began to move and the shape of the bank remained the same, which satisfies the moderate restarting status. The pump rate at this moment was 154.83 kg/h, which is equivalent to 0.000091 m^3/s. The height of the sand bank was calculated based on the image analysis performed by the i-SPEED control software. The center of the window was located based on the edge of the window. The sand bank height was then calculated based on the distance between the window center and the sand bank surface. In Figure 3, the sand bank has a height of 26.01 mm, which is approximately half the height of the simulated channel.

3.2 Empirical equation for the particle restarting pump rate in SC-CO_2

An empirical equation for the particle restarting pump rate was fitted based on the Shields number, which is commonly used as a criterion for particle restarting status in conventional fluids. The particle restarting Shields number for each group of experiments was calculated using the data in Table 1.

The general expression for the Shields number is [19]

$$S = \frac{\tau_c}{(\rho_p - \rho_f) g d_p} \tag{1}$$

where τ_c is the drag force acting on a particle, ρ_f is the density of SC-CO_2, ρ_p is the density of the particles, d_p is the diameter of a particle, and g is the force of gravity.

According to the rolling theory of particle restarting, the drag force generated by the flowing fluid is the main driving force [11]. The drag force acting on a surface particle is defined as

$$\tau_c = \mu\gamma \tag{2}$$

where μ is the viscosity of SC-CO_2, and γ is the shear velocity.

For the channel flow, the shear velocity can be written as

$$\gamma = \frac{8Q}{w^2(H-h)} \tag{3}$$

where Q is the pump rate, w is the width of the fracture, H is the height of the fracture, and h is the height of the sand bank.

By substituting Eqs. (2) and (3) into Eq. (1), the Shields number for particle restarting in the channel flow can be calculated as

$$S = \frac{8\mu Q}{(\rho_p - \rho_f)gd_p w^2(H-h)} \tag{4}$$

The Shields numbers were calculated using Eq. (4) based on the experimental data in Table 1. The density and viscosity of SC-CO_2 were taken from the National Institute of Standards and Technology website [20]. The experimental density of SC-CO_2 in this work fell in the range of 217.46–672.34 kg/m^3. The viscosity fell in the range of 0.020–0.0529 mPa·s. These values of density and viscosity are close to the actual values under the reservoir temperature and pressure conditions. For example, the density and viscosity of SC-CO_2 under the formation conditions of 30 MPa and 100 °C are 661.87 kg/m^3 and 0.0540 mPa·s, respectively. Therefore, the particle restarting behaviors in SC-CO_2 under the experimental conditions are close to the behaviors under actual formation conditions.

The calculated Shields numbers for SC-CO_2 were 0.0026, 0.0034, 0.0015, 0.0036, 0.0040, 0.0017, 0.0032, 0.0028, and 0.0028. The average value is 0.0028, which is considered to be the critical

Shields number when particles achieve the moderate restarting status in SC-CO_2. When the Shields number has a value of 0.0028, the Eq. (4) can be rewritten as

$$Q = \frac{0.00035(\rho_p - \rho_f) g d_p w^2 (H - h)}{\mu} \tag{5}$$

Eq. (5) is the empirical equation for the particle restarting pump rate in SC-CO_2, which can be used for the optimization of hydraulic parameters (proppant selection and pump rate) during engineering design. Using density as a constraint condition, the valid density of SC-CO_2 for this equation ranges from 217.46 to 672.34 kg/m^3 (the viscosity of SC-CO_2 can also be used as a constraint condition because the density and viscosity of SC-CO_2 have the same trends of increase and decrease).

It is worth noting that the measured Shields numbers for SC-CO_2 falls in the range of 0.0015–0.0040. These are relatively small values. According to Eq. (1), the Shields number is the ratio between the drag force and effective gravity (gravity minus buoyancy). The smaller the Shields number is, the smaller the drag force required to drive the particle restarting. Apparently, the particle restarting status is easily achieved in SC-CO_2 under the experimental conditions presented in this paper. Further analysis elucidates the particle restarting behaviors in SC-CO_2 by analyzing the forces acting on restarting particle.

3.3 Forces operating on restarting particles in SC-CO_2

Analysis of the forces operating on particles elucidated the particle restarting behaviors in SC-CO_2. The particle restarting process was divided into two stages according to the force characteristics: the initial stage, where particles roll on the surface of the sand bank and the bouncing stage, where particles separate from the surface of the sand bank.

3.3.1 Force analysis during the initial stage

According to the rolling theory, a surface particle is dragged by a drag force (F_D) and resisted by effective gravity (G) and the cohesive force (F_C) between particles, as shown in Figure 4. Particle M begins to pivot on point P when the drag force torque, effective gravity torque, and cohesive force torque are balanced.

The expression for drag force is written as

$$F_D = \frac{\pi d_p^2}{8} \rho_f \upsilon_f{}^2 C_d \tag{6}$$

where d_p is the particle diameter, ρ_f is the density of SC-CO_2, υ_f is the velocity of SC-CO_2, and C_d is the drag coefficient. According to Eq. (6), the drag force acting on a restarting particle is affected by the density of the fluid and the drag coefficient. The density differentiation is significantly larger than the drag coefficient differentiation [21]. Therefore, fluid density has a larger contribution to drag force than the drag coefficient [18]. The density of SC-CO_2 is two orders of magnitude larger than that of gaseous CO_2, and is close to that of liquid CO_2. Therefore, the value of the drag force acting on restarting particles in SC-CO_2 is close to that acting on restarting particles in liquid CO_2.

The cohesive force is one of the main resistance forces. This force exists in all liquids and is caused by surface tension. There is a thin layer of water film covering the particle surfaces that is created by surface tension. When the distance between particles is sufficiently small, a shared water film is formed between particles based on compression. The cohesive force is the resistance force generated when the particles are separated and the shared water film is divided [22,23]. The strength of the cohesive force is approximately 25 % of the force of gravity for a particle with a diameter in the range of 0.1–1.0 mm in water [24]. Additionally, the smaller the particle, the more significant the influence of the cohesive force in terms of hindering particle restarting. However,

the cohesive force in SC-CO_2 is zero based on its non-surface-tension characteristic. In other words, a restarting particle in SC-CO_2 faces approximately 25 % less resistance than a restarting particle in water.

Force analysis revealed that the drag force (main driving force) acting on restarting particles in SC-CO_2 is close to that in liquid CO_2. Additionally, the cohesive force (main resistance other than gravity) is zero. In the initial stage of restarting, particles in SC-CO_2 easily achieve the restarting status because of the relatively large drag force and negligible cohesive force. This analysis result agrees with the experimental results.

3.3.2 Force analysis in the bouncing stage

The restarting particles roll on the surface of the sand bank during the initial stage and then are separated from the surface during the bouncing stage. During this period, the Magnus force and buoyancy in the vertical direction act against gravity and slow the particle settling velocity, which increases the transportation distance of the particles. Buoyancy has been proven to a have significant effect on settling particles in SC-CO_2 [18]. The Magnus force exhibits significantly different values in gases and liquids. In gases, the particle rotation speed can reach as high as 100–1000 r/s. The value of the Magnus force under this rotation speed is approximately 20 % of the force of gravity, which enhances the bouncing height and distance [25]. In liquids, the particle rotation speed is generally less than 45 r/s, indicating that the Magnus force is negligible [26].

The value of the Magnus force in SC-CO_2 is determined by the particle rotation speed, which was measured under the conditions listed in Table 1. The particle restarting experiment in SC-CO_2 under pressure and temperature conditions of 42.7 °C and 9.42 MPa, respectively, was considered as an example. The particle rotation speed was recorded, as shown in Figure 5. It took 0.0040 s for

a particle to rotate 180° (0.5 r), meaning the particle had a rotation speed of 125 r/s. Ninety additional particles were chosen randomly. The measured rotation speeds ranged between 70 and 560 r/s and had an averaged value of 121 r/s. The measurement error (particles spin in three dimensions, but the high-speed camera only records images in two dimensions) and significant randomness of particle shapes and impacts resulted in a wide range of rotation speeds. However, the averaged value indicates that particles have the same spinning speed in SC-CO_2 as they do in gases.

The Magnus force has a significant effect on particle restarting under high rotation speeds. When considering the gravity, buoyancy, drag force, and Magnus force, the particle vertical motion differential equation can be written as

$$\frac{\pi d_p^3}{6}\rho_p\frac{d\upsilon_p}{dt}=\frac{\pi d_p^3}{6}\rho_p g-\frac{\pi d_p^3}{6}\rho_f g-\frac{\pi d_p^2}{8}\rho_f\upsilon_p^2 C_d-\frac{\pi d_p^3}{8}\rho_f\upsilon_p\omega \tag{7}$$

The drag coefficient (C_d) is calculated using the following auxiliary equations [21].

$$\begin{cases} C_D=\dfrac{4g(\rho_p-\rho_f)d_p}{3\upsilon_\infty^2\rho_f} \\ \upsilon_\infty=\dfrac{\mu}{\rho_f d_p}[0.1196(\dfrac{\rho_p}{\rho_f})^2-0.1216\dfrac{\rho_p}{\rho_f} \\ \qquad -0.2961]Ar^{[-0.214\ln(\frac{\rho_p}{\rho_f})+0.8241]} \end{cases} \tag{8}$$

By combining Eqs. (7) and (8), a particle vertical motion model was constructed and solved using Runge–Kutta method [27] for forces analysis. This model was verified in a previous study [18]. The calculation program was written in VB.net. The spinning particle in Figure 5 was considered as an example. The particle diameter and density were 0.647 mm and 3120 kg/m^3, respectively. The SC-CO_2 temperature and pressure were 42.7 °C and 9.42 MPa, respectively. The forces acting on the restarting particle calculated by the vertical motion model are shown in Figure 6. Apparently, a force balance was achieved after a short period of acceleration (approximately

0.03 s). The buoyancy force was not negligible and had a value as large as 15 % of the force of gravity. The Magnus force (nearly one third of the force of gravity) played a key role in hindering the particle settlement in the SC-CO_2. Furthermore, the ratios of the Magnus force to the gravitational force under various rotation speeds were analyzed under the same particle and SC-CO_2 conditions, as shown in Figure 7. The ratios all fall in the range of 0.26–0.57.

4. Conclusions

In this work, particle restarting behaviors in SC-CO_2 were studied by introducing the theories of sand dynamics and river sediment dynamics into the petroleum engineering field. Both experimental simulations and force analyses were performed. An empirical equation for the particle restarting pump rate in SC-CO_2 was fitted based on the experimental results. This equation can be used for the optimization of hydraulic parameters, such as proppant selection and pump rate. The measured particle Shields numbers fell in the range of 0.0015–0.0040 with an average value of 0.0028. The smaller the Shields number, the smaller the drag force required to drive particle restarting. Additional force analysis indicated that the drag force (main driving force) acting on restarting particles in SC-CO_2 is similar to that acting on particles in liquid CO_2. Additionally, the cohesive force (main resistance force) between particles in SC-CO_2 is zero based on its non-surface-tension characteristic. Furthermore, the averaged rotation speed of particles in SC-CO_2 is 121 r/s according to our measurements. The Magnus force induced by the high-speed rotation is approximately 30 % of the force of gravity, which decreases the particle settlement and increases transportation distance. By synthesizing the features of the Shields number, drag force, cohesive force, and Magnus force, particles in SC-CO_2 was determined to be easy to restart.

Acknowledgements

This research is supported by the National Natural Science Foundation of China (Project No. 51490653, No. U1562212), National Science and Technology Major Project (No. 2016ZX05061, No. 2017ZX05005), and SINOPEC Ministry of Science and Technology Project (No. P17014-6).

References

[1] X. Li, D. Elsworth, Geomechanics of CO_2 enhanced shale gas recovery, J. Natural Gas Science & Eng. 26 (2014) 1607–1619.

[2] X. Luo, S. Wang, Z. Wang, Z. Jing, M. Lv, Z. Zhai, T. Han, Experimental investigation on rheological properties and friction performance of thickened CO_2 fracturing fluid, J. Petroleum Science and Eng. 133 (2015) 410–420.

[3] Yang, J., Wang, Y., Chen, J., Feng, G., Wang, J, Adaptive finite element–discrete element analysis for the multistage supercritical CO2 fracturing and microseismic modelling of horizontal wells in tight reservoirs considering pre-existing fractures and thermal-hydro-mechanical coupling, J. Natural Gas Science & Eng. 61 (2019) 251–269.

[4] L. Hou, B. Sun, X. Geng, T. Jiang, Z. Wang, Study of the slippage of particle/supercritical CO_2 two–phase flow, J. Supercritical Fluids 120 (2017) 173–180.

[5] S. Y. Tong, K. K. Mohanty, Proppant transport study in fractures with intersections, Fuel 181 (2016) 463–477.

[6] A. Raimbay, T. Babadagli, E. Kuru, K. Develi, Quantitative and visual analysis of proppant transport in rough fractures, J. Natural Gas Science & Eng. 33 (2016) 1297–1307.

[7] E. V. Dontsov, A. P. Peirce, Proppant transport in hydraulic fracturing: Crack tip screen–out in KGD and P3D models, Int. J. Solids Struct. 63 (2015) 206–218.

[8] M. Arshadi, M. Piri, M. Sayed, Proppant-packed fractures in shale gas reservoirs: An in-situ

investigation of deformation, wettability, and multiphase flow effects, J. Natural Gas Science & Eng. 59 (2018) 387–405.

[9] J. Wang, D. D. Joseph, N. A. Patankar, M. Conway, R.D. Barree, Bi–power law correlations for sediment transport in pressure driven channel flows, Int. J. Multiphase Flow 29 (2003) 475–494.

[10] S. Shiozawa, M. McClure, Simulation of proppant transport with gravitational settling and fracture closure in a three–dimensional hydraulic fracturing simulator, J. Petrol. Sci. Eng. 138 (2016) 298–314.

[11] Z. B. Dong, W. Y. Luo, Comparable analysis of force balance model for the wind initiation threshold for particles on sandy bed, Journal of Desert Research 27 (2007) 356–361.

[12] X. J. Zhen, L. Xie, X. Y. Zou, The effect of electrostatic force on the evolution of sand saltation cloud, The Europen Physical Jornal E. 19 (2006) 129–138.

[13] V. Etyemezian, G. Nikolich, W. Nickling, J. S. King, J. A. Gillies, Analysis of an optical gate device for measuring aeolian sand movement, Aeolian Research, 24 (2017) 65–79.

[14] X. Yin, N. Huang, Z. S. Wang, A numerical investigation into sand grain / slope bed collision, Power Technology 314 (2017) 28–38.

[15] H. Karmer, Sand mixtures and sand movement in fluvial model, Trans. ASCE 100 (1935) 798–838.

[16] M. Ouriemi, P. Aussillous, M. Medale, Determination of the critical shields number for particle erosion in laminar flow, Physics of Fluids, 19 (2007) 061706–061710.

[17] Y. K. Du, R. H. Wang, H. J. Ni, W. Q. Song, H. F. Song, M. K. Li, Determination of rock-breaking performance of high-pressure supercritical carbon dioxide jet, J. Hydrodynamics 24

(2012) 554–560.

[18] L. Hou, T. X. Jiang, H. Liu, X. Y. Geng, B. J. Sun, G. S. Li, S. W. Meng, An evaluation method of supercritical CO_2 thickening result for particle transporting, J. CO_2 Util. 21 (2017) 247–252.

[19] J. F. Kennedy, The Albert Shields story, Journal of Hydraulic Engineering 121 (1995) 766–772.

[20] National Institute of Standards and Technology. NIST Chemistry WebBook, 2014, Available from: http://webbook.nist.gov/chemistry/fluid

[21] L. Hou, B. J. Sun, Z. Y. Wang, Q. J. Li, Experimental Study of Particle Settling in Supercritical Carbon Dioxide, J. of Supercritical Fluids 100 (2015) 121–128.

[22] L. D. Zhang. Study on Starting Velocity of Cohesive Sediment, Journal of Hydrodynamics 15 (2000) 82–88.

[23] R. Kriby, W. R. Parker, Distribution and behavior of fine sediment in the Severn estuary and inner Bristol Channel, Canadian Journal of Fisheries and Aquatic Science 40 (1983) 83–95.

[24] S. Q. Li, Y. J. Lu, L. Q. Zuo, Incipient sediment motion in steady boundary layers, Advances in Water Science 24 (2013) 821–829.

[25] B. Yang, X. Y. Zou, Mechanical analysis of a single saltating particle in air flow, Scientia Geographica Sinica 19 (1999) 475–478.

[26] Q. Q. Liu, W. H. Cao, On the mechanism of winnowing of sediment particles, SHUI LI XUE BAO 5 (1998) 1–6.

[27] F.A. Bombardelli, A.E. González, Y.I. Niño, Computation of the particle basset force with a fractional-derivative approach, J. Hydraulic Eng. 134 (2008) 1513–1519.

Figure List

Fig. 1 Schematic of the visualization channel simulator and high-speed camera system

Fig.2 The observation of the sand bank through the window

Fig.3 The moment of particles restarting in SC-CO_2. The temperature and pressure of SC-CO_2 were 42.7 °C and 9.42 MPa, respectively. The density and averaged diameter of particle were 3120 kg/m^3 and 0.45 mm, respectively. The pump rate of SC-CO_2 was 154.83 kg/h (0.000091 m^3/s) at this moment. The flowing direction was from left to right.

Fig.4 The schematic of forces acting on the restarting particle in the initial stage. Particle M starts to pivot on point P when the drag force (F_D) torque, effective gravity (G) torque and cohesive force (F_C) torque achieve a balance.

Fig.5 Experimental observations of particle rotating in SC-CO_2. The temperature and pressure of SC-CO_2 are 42.7 ℃ and 9.42 MPa, respectively. The density and averaged diameter of particle are 3120 kg/m3 and 0.647 mm, respectively. The pump rate of SC-CO_2 is 154.83 kg/h (0.000091 m^3/s). The flowing direction was from left to right.

Fig.6 Vertical forces acting on the bouncing particle using the motion model. Calculation conditions: The particle diameter and density were 0.647 mm and 3120 kg/m^3, respectively. The SC-CO_2 temperature and pressure were 42.7 °C and 9.42 MPa, respectively.

Fig.7 The ratio of Magnus Force and gravity under various rotation speeds. Calculation conditions: The particle diameter and density were 0.647 mm and 3120 kg/m^3, respectively. The SC-CO_2 temperature and pressure were 42.7 ℃ and 9.42 MPa, respectively.

Figure
Click here to download high resolution image

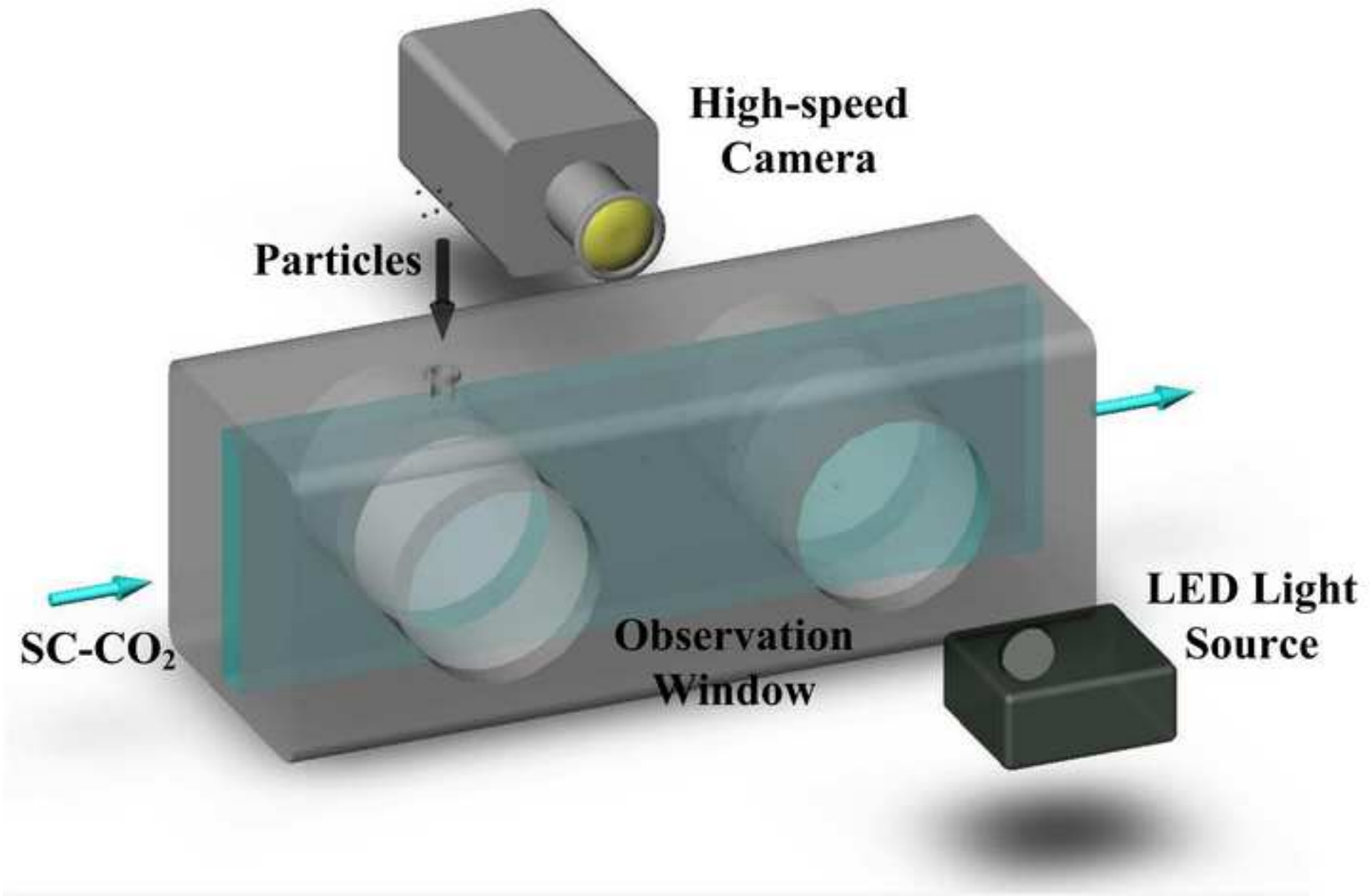

Figure

Click here to download high resolution image

Figure

Click here to download high resolution image

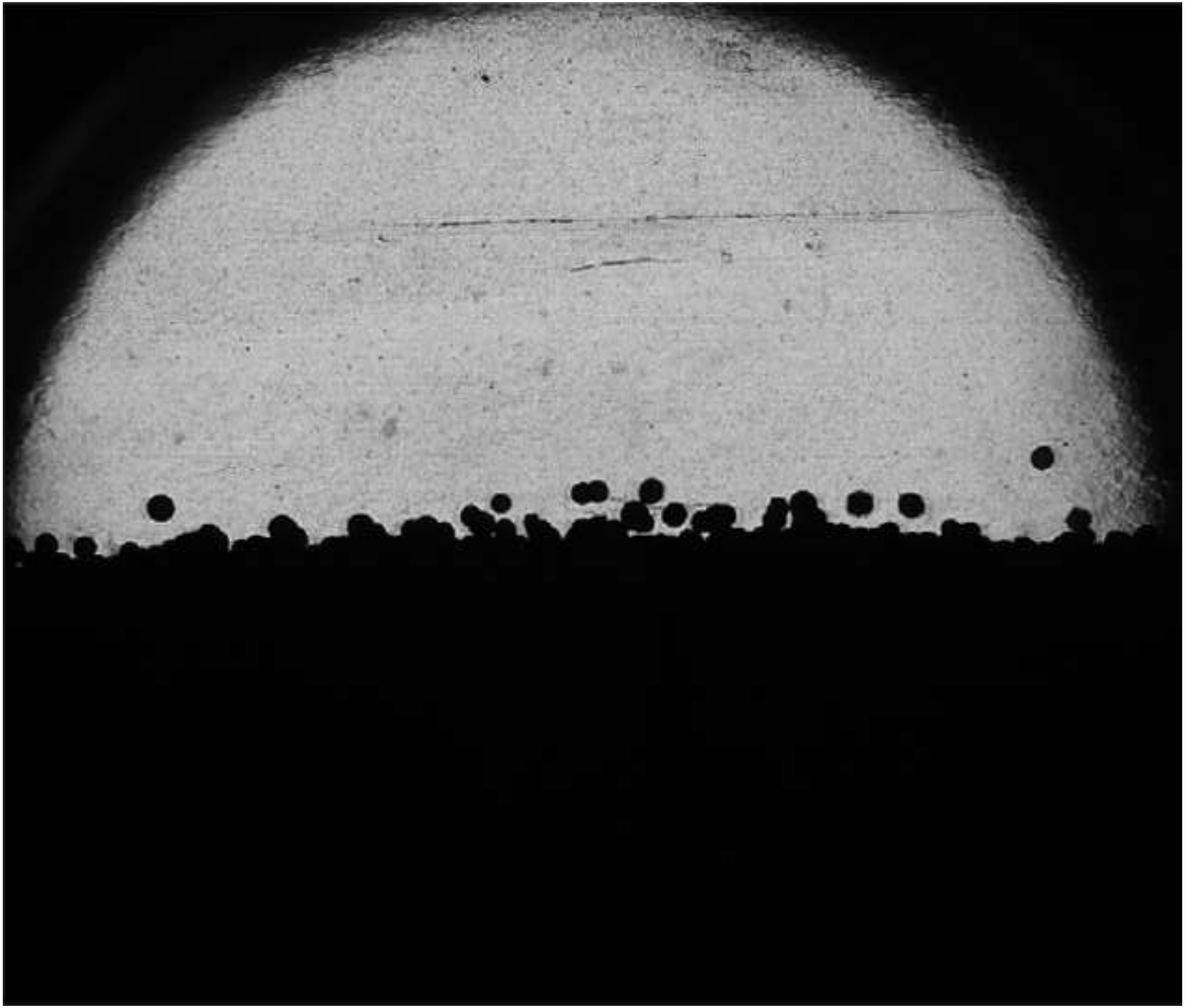

Figure

Click here to download high resolution image

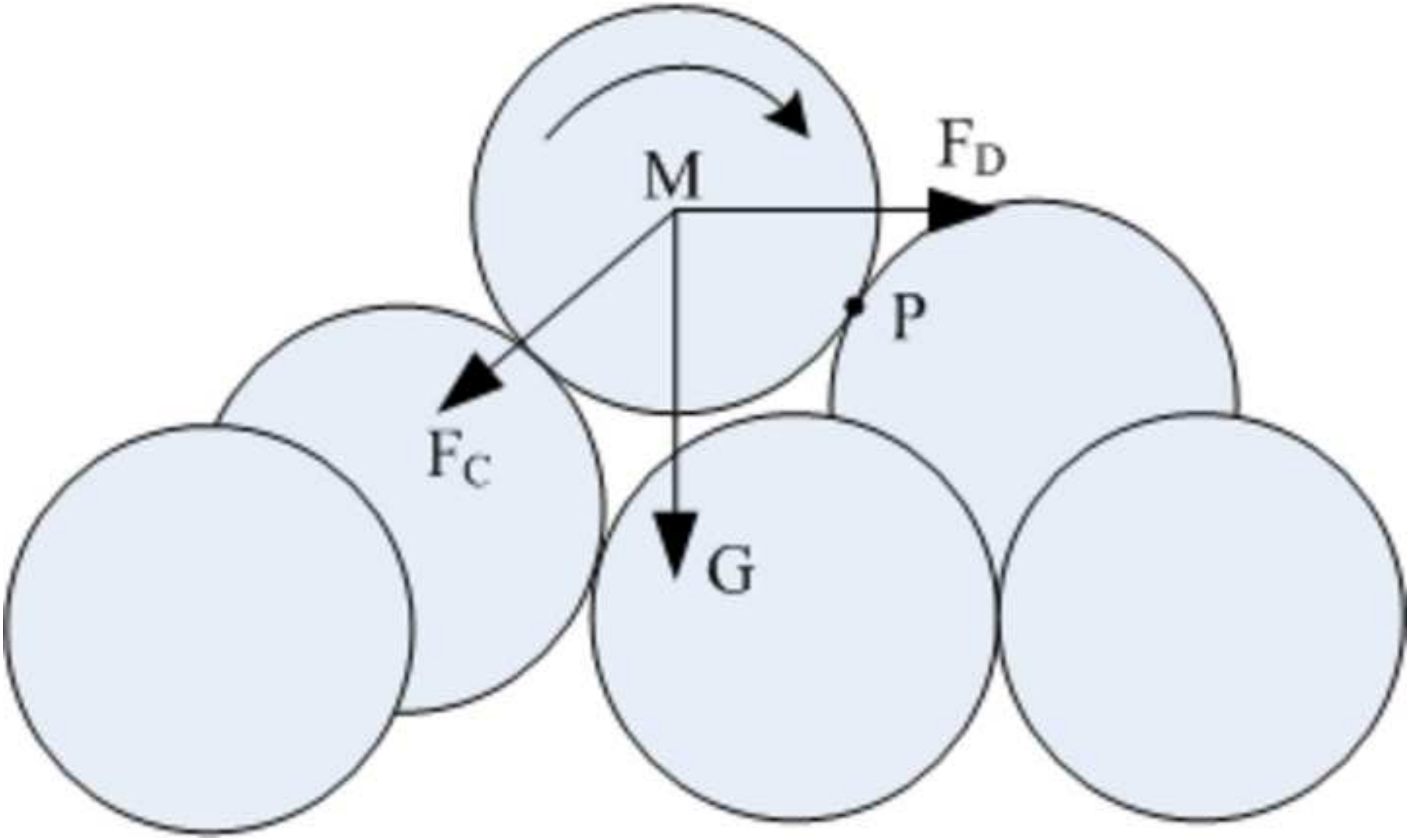

Figure

Click here to download high resolution image

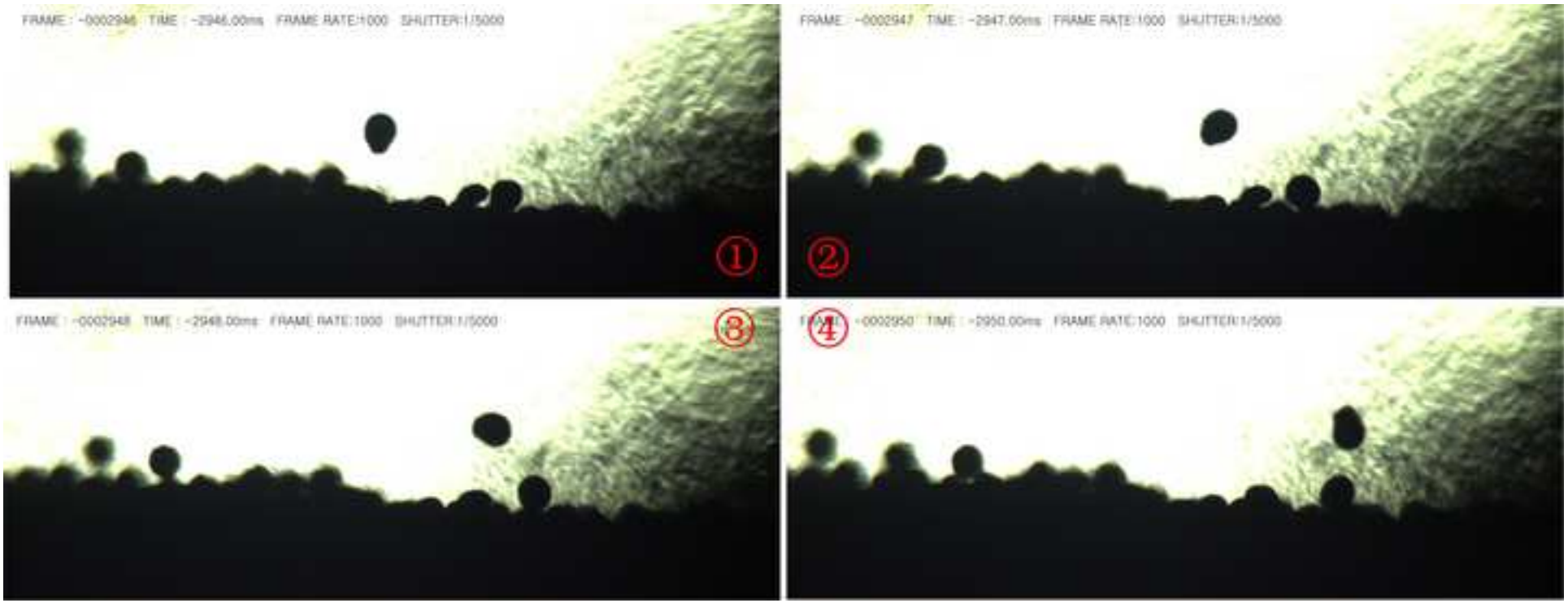

Figure

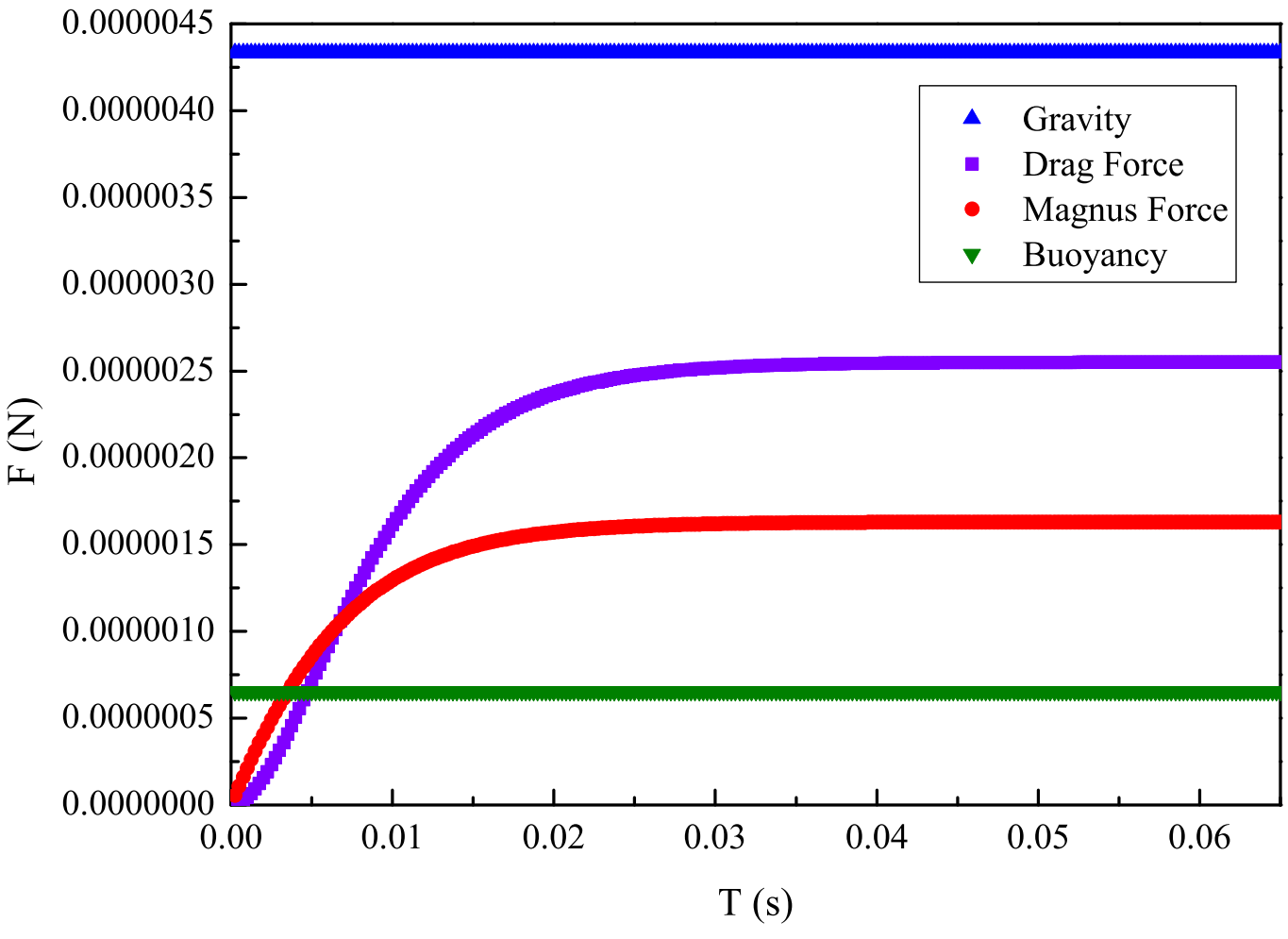
0.0000045
0.0000040
0.0000035
0.0000030
0.0000025
0.0000020
0.0000015
0.0000010
0.0000005
0.0000000
F (N)
0.00
0.01
0.02
0.03
0.04
0.05
0.06
T (s)
Gravity
Drag Force
Magnus Force
Buoyancy

Figure

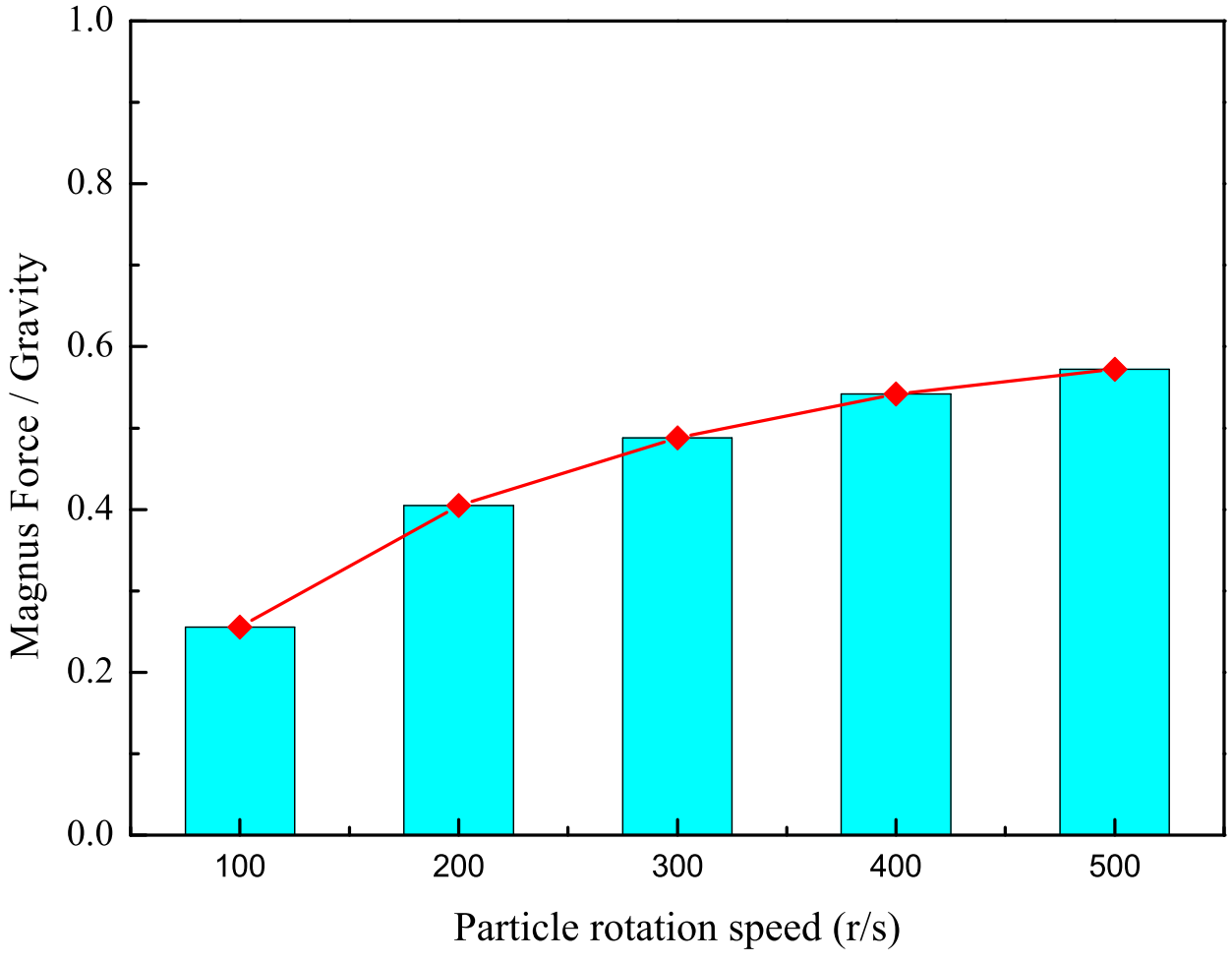
1.0
0.8
0.6
0.4
0.2
0.0
Magnus Force / Gravity
100
200
300
400
500
Particle rotation speed (r/s)

Table

Table 1 Experimental conditions and results of particle restarting in SC-CO_2

	Temperature ℃	Pressure MPa	SC-CO_2 density kg/m³	SC-CO_2 viscosity cp	Particle density kg/m³	Averaged particle diameter mm	Flowing height（H-h） mm	Restarting pump rate m^3/s	Shields number
1	38.1	7.84	279.91	0.0223	3120	0.44	30.12	0.000134	0.0026
2	41.1	7.38	217.46	0.020	3120	0.44	30.69	0.000203	0.0034
3	38.4	7.96	292.07	0.0229	3120	0.44	22.65	0.000057	0.0015
4	42.7	9.42	470.68	0.0338	3120	0.44	23.99	0.000091	0.0036
5	41.5	8.87	390.63	0.0283	3120	0.44	26.38	0.000137	0.0040
6	37.2	7.59	259.87	0.0214	2630	0.63	14.21	0.000050	0.0017
7	40.4	9.41	554.16	0.0405	2630	0.63	28	0.000088	0.0032
8	43.2	11.78	672.34	0.0529	2630	0.63	33.4	0.000066	0.0028
9	41.2	10.04	605.48	0.0455	2630	0.63	26.66	0.000064	0.0028